BBA - Molecular Basis of Disease 1871 (2025) 167842

Contents lists available at ScienceDirect

BBA - Molecular Basis of Disease

journal homepage: www.elsevier.com/locate/bbadis

Proteome alterations in peripheral immune cells of DLBCL patients and evidence of cancer extracellular vesicles involvement

Mostafa Ejtehadifar [a], Sara Zahedi [a], Paula Gameiro [b], José Cabeçadas [b], Manuel S. Rodriguez [c], Maria Gomes da Silva [b], Hans Christian Beck [d], Rune Matthiesen [a,*,1], Ana Sofia Carvalho [a,*,1]

[a] iNOVA4Health, NOVA Medical School, Faculdade de Ciências Médicas, Universidade NOVA de Lisboa, Lisboa, Portugal
[b] Instituto Português de Oncologia, Departament of Hematology, Lisbon, Portugal
[c] Laboratoire de Chimie de Coordination (LCC) - UPR 8241 CNRS, UMR 152 Pharma-Dev, Université de Toulouse, IRD, UPS, 31400 and BMolecular, Centre Pierre Potiers, 31100 Toulouse, France
[d] Centre for Clinical Proteomics, Department of Clinical Biochemistry, Odense University Hospital, DK-5000 Odense C, Denmark

ARTICLE INFO

Keywords:
Peripheral immune cells
Diffuse large B cell lymphoma
Extracellular vesicles
Proteomics
Polyubiquitination

ABSTRACT

Diffuse large B-cell lymphoma (DLBCL) is an aggressive disease and a frequent form of non-Hodgkin lymphoma. Given the primary localization of DLBCL and the effect of tumors on the systemic immune response, we investigated the proteome of DLBCL patients' and healthy donors (HDs') peripheral immune cells (PICs). Since the ubiquitin-proteasome system has a vital role in proteome regulation and immune cells' functions, this study also explores the potential impact of DLBCL secretome on the polyubiquitination level in PICs. PICs from DLBCL patients and HDs were isolated and analyzed by mass spectrometry-based proteomics. The analysis resulted in 135 down and 51 upregulated proteins (adjusted p-value <0.05). Unsupervised principal component analysis revealed distinct proteomic profiles between DLBCL and HDs. Functional enrichment analysis for comparison between DLBCL and HDs-PICs proteome identified immune-related pathways such as innate immune system, specifically neutrophil degranulation, Fcγ receptor-dependent phagocytosis, and JAK-STAT signaling after IL-12 stimulation as downregulated. Proteomics analysis of DLBCL-PICs also showed dysregulation of proteostasis factors. This prompted the investigation of the effect of tumor secretome on viability and polyubiquitination level in mononuclear immune cells. Therefore, human HD peripheral blood mononuclear cells (PBMCs) were cultured in the presence of DLBCL cell line-derived soluble factors, small-EVs, and large-EVs in vitro. Our results revealed that exposure of mainly small-EVs, and large-EVs to HD PBMCs increased the polyubiquitination in PBMCs and decreased PIC viability. These findings suggest impaired immune responses in DLBCL-PICs, with tumor secretome-inducing polyubiquitination and reduced PIC viability.

1. Introduction

Diffuse large B-cell lymphoma (DLBCL) is an aggressive disease and the most common entity among all subtypes of non-Hodgkin lymphoma [1]. DLBCL patients are treated with R-CHOP (rituximab, cyclophosphamide, doxorubicin, vincristine, prednisone) and derivative regimens, with favorable outcomes in 60–70 % of the cases [2]. According to gene expression profiling, DLBCL is categorized into two main molecular subgroups: germinal center B-cell-like (GCB), and activated B-cell-like (ABC), with 10–15 % of cases remaining unclassifiable [3]. In immunohistochemistry-based analysis, non-classifiable and ABC subtypes constitute the non-GCB subgroup. Like a double-edged sword, immune cells within the tumor microenvironment (TME) can either support or suppress tumor growth by inhibiting or inducing responses and promoting infiltration of other immune cells into the TME [4–7]. In the TME, immune cells such as T-cells, B-cells, macrophages (M1 and M2), and neutrophils are in close contact with DLBCL tumor cells [8,9] and may have prognostic values in non-Hodgkin lymphoma [10–13]. Recent studies demonstrated that both the presence and specific classes of T-cells within the lymphoma TME are associated with patient prognosis [4,14]. Previous efforts attempted to evaluate the clinical impact of the TME by considering associations between distinct immune cell

* Corresponding authors.
E-mail addresses: rune.matthiesen@nms.unl.pt (R. Matthiesen), ana.carvalho@nms.unl.pt (A.S. Carvalho).
[1] These authors contributed equally to this work and share last authorship.

https://doi.org/10.1016/j.bbadis.2025.167842
Received 13 January 2025; Received in revised form 14 March 2025; Accepted 8 April 2025
Available online 11 April 2025

subtypes within the TME and patients' survival, although the results obtained were controversial [15–19].

Given the role of infiltrating peripheral immune cells (PICs) in shaping the TME, previous studies have investigated the relationship between the ratios of these immune cell populations and DLBCL outcomes [11,20,21]. The distribution of immune cell subpopulations within the TME has been linked to the systemic leakage of various factors into the bloodstream. These include cytokines, chemokines, and extracellular vesicles (EVs), all of which possess the capacity to modify and attract immune cells from the peripheral blood [22]. Tumor-derived EVs can directly induce immune suppression by transporting signals that either suppress immune responses or trigger apoptosis in activated immune cells [23]. Furthermore, we previously demonstrated that EV proteome from DLBCL patients compared to controls are significantly different [24]. Mechanistically, gastric cancer derived EVs increased the expression of E3 ubiquitin ligases Cbl-b and c-Cbl of T cells in time and concentration dependent manner [25]. In light of this, we hypothesized that the subpopulations of immune cells in the blood circulation of diffuse large B-cell lymphoma (DLBCL) patients differ not only in composition but also in their proteomic profiles, potentially offering diagnostic value and insights into how DLBCL interacts with the immune system. Accordingly, this study first investigates the proteome differences between the immune cells of DLBCL patients and those from a healthy control group. Considering the critical roles that peripheral blood mononuclear cells (PBMCs), such as lymphocytes and monocytes, play in shaping the immune composition within the TME and their enduring anti-tumor functions, especially when compared to polymorphonuclear cells like neutrophils, the second phase of this study aims to explore how DLBCL cells affect PBMCs. The interactions between immune and cancer cells occur through various mechanisms, including complex molecular signaling pathways, direct cell-to-cell communication, and the exchange of soluble factors, all of which have been extensively studied [26]. Previous studies demonstrated that EVs, released from cancer cells can affect both monocytes and lymphocytes. For instance, CLL and DLBCL augment the CD8+ T cells activities [27] and M2 polarization of macrophages [28] in TME. The ubiquitin-proteasome system (UPS), known for its essential roles in immune cells [29], is potentially affected by tumor cells, yet the specific effects of DLBCL tumor cells on PBMCs have remained largely unexplored. Therefore, in the second phase of the current study, the role of the DB cell line derived EVs on polyubiquitination level in PBMCs is studied. To date, the questions surrounding the effects of DLBCL tumor cells on PICs and the mechanisms through which these effects are transferred from tumor cells to PICs as well as PICs' diagnostic potential remain unanswered. Therefore, this study focused on the proteome profile of PICs from DLBCL and healthy donors (HDs) and performed functional in vitro assays using PICs from HDs by exposing them to tumor small EVs (sEVs), large EVs (lEVs), and soluble factors (SFs).

2. Material and methods

2.1. DLBCL patients and healthy donor cohort

The study was approved by the Human Ethics Committee of NOVA Medical School (n°146/2021/CEFCM) and Instituto Português de Oncologia de Lisboa Francisco Gentil (UIC/1174) before initiation of blood collection. Peripheral blood was prospectively collected from patients diagnosed with DLBCL in IPOLFG, Portugal, between May 2018 and January 2020. All participants in the study signed the informed consent and processes on human samples were performed per the 1964 Helsinki Declaration. In total samples from 10 HDs and 10 patients (non-GCB $n = 5$ and GCB n = 5) were selected for analysis (Tables 1 and 2).

According to the Hans algorithm, immunohistochemistry assessment of the corresponding formalin-fixed paraffin-embedded DLBCL biopsies was performed to diagnose and sub-classify patients. Noteworthy, peripheral blood samples were obtained from all DLBCL patients before first-line treatment.

Table 1
Overview of study subjects. N/n indicates the number of subjects in total and each subgroup, respectively.

Variable	N	GCB, $n = 5$[a]	HD, $n = 10$[a]	Non-GCB, n = 5[a]	p-Value[b]
Status	20				<0.001
DLBCL		5 (100 %)	0 (0 %)	5 (100 %)	
HD		0 (0 %)	10 (100 %)	0 (0 %)	
Age (years)	20	61 (61, 65)	58 (56, 59)	61 (60, 67)	0.022
Gender	20				0.4
F		2 (40 %)	7 (70 %)	2 (40 %)	
M		3 (60 %)	3 (30 %)	3 (60 %)	

[a] n (%); Median (inter quartile range, IQR).
[b] Fisher's exact test; Kruskal-Wallis rank sum test.

Table 2
Clinical characteristics of DLBCL participants. n indicates the number of subjects in each subgroup.

		Subtype		
Variable	n	GCB, $n = 5$[a]	Non-GCB, n = 5[a]	p-Value[b]
Age (years)	10	63.40 (4.16)	62.60 (4.16)	0.7
Gender	10			>0.9
F		2 (40 %)	2 (40 %)	
M		3 (60 %)	3 (60 %)	
IPI	10			0.8
1		1 (20 %)	1 (20 %)	
2		1 (20 %)	3 (60 %)	
3		2 (40 %)	0 (0 %)	
4		1 (20 %)	1 (20 %)	
Lactate Dehydrogenase (U/L)	10	682 (1038)	245 (135)	0.7
Hemoglobin (g/dL)	10	15.28 (1.70)	12.84 (2.18)	0.10
Leukocytes (cells/L)	10	13,396 (11,331)	8858 (4536)	0.7
Lymphocytes (cells/L)	10	1920 (1179)	1994 (1557)	>0.9
Neutrophils (cells/L)	10	9440 (7643)	6110 (4202)	0.5
Monocytes (cells/L)	10	668 (336)	568 (368)	0.8
Platelets (cells/L)	10	215 (67)	327 (132)	0.2
Albumin (g/dL)	9	4.2 (0.5)	3.9 (0.8)	0.7

[a] Mean (standard deviation, SD); n (%).
[b] Wilcoxon rank sum test; Fisher's exact test; Wilcoxon rank sum exact test.

2.2. Buffy coat isolation

Peripheral blood samples from HDs and treatment naïve DLBCL patients were collected into EDTA collection tubes and then immediately centrifuged at 200 ×*g* for 10 min at RT. The top layer corresponding to plasma was collected and centrifuged at 1000 ×*g* for 10 min. The intermediate layer containing white blood cells was collected and washed twice with red blood cell lysis buffer at 300 ×*g* for 10 min to remove the remaining red blood cells. Lastly, pelleted leukocytes were resuspended in PBS to remove any lysis reagent by centrifugation at 300 ×*g* for 5 min. Cleared leukocyte pellets were stored at −80 °C until further use (maximum storage time 1 year).

2.3. Peripheral blood mononuclear cell isolation

PBMCs were isolated and cultured for in vitro functional studies. PBMCs were isolated by density gradient separation from HDs in EDTA blood collection tubes. Briefly, mixed blood with an equal volume of PBS was layered over 10 mL of Biocoll 1.077 (Merck) by gently pipetting and centrifuged for 30 min at 1200 ×*g*, 22 °C with no break. PBMCs at the interface were collected and washed twice with 20 mL PBS by centrifugation at 700 ×*g*, for 10 min.

2.4. Cell culture, EV, and condition medium preparation

DB (ACC-539) cell line was purchased from Leibniz Institute DSMZ (German Collection of Microorganisms and Cell Cultures, Braunschweig, Germany) and was cultured following supplier instructions. Cells were tested for mycoplasma contamination and were cultured in RPMI-1640 medium supplemented with 20 % FBS, 100 U/mL Penicillin, and 100 μg/mL Streptomycin (Gibco, Invitrogen, Waltham, MA, USA) at 37 °C in 5 % CO_2. DB conditioned media (CM) was harvested from the initial culture of 2.5×10^5 cells/mL after 48 h. CM was centrifugated at 300 ×*g* for 5 min at 4 °C to pellet down the cells, and CM was stored at −20 °C. Ultracentrifugation was used to isolate EVs as follows.

2.5. EV isolation and characterization

To isolate EVs, 15×10^6 cells from DB cell line were washed with PBS and then cultured for 48 h in RPMI-1640 medium supplemented with 20 % EV-depleted FBS, 100 U/mL Penicillin, and 100 μg/mL Streptomycin (Gibco) at 37 °C in 5 % CO_2. After incubation time, the medium containing EVs was collected by 300 ×*g* centrifugation for 5 min at 4 °C. The supernatant was centrifuged for 20 and 60 min in 3000 ×*g* and 12,000 ×*g*, respectively. In this step, we collected lEVs by using 500 μL of ice-cold PBS. The supernatant of the previous step was centrifuged at 100,000 ×*g* for 120 min at 4 °C with a type 32.1 Ti rotor (k-factor:229) in a Beckman Coulter Optima (L-90K). The supernatant of the step was collected and stored at −80 °C as the EVDCM. sEVs were re-suspended in ice-cold PBS. Both lEVs and sEVs were stored at −80 °C.

A NanoSight NS300 instrument (Malvern Panalytical, Malvern, UK) was used to determine the concentrations and sizes of the EVs in the samples. Samples were diluted in PBS to a final volume of 1 mL to reach the ideal particle concentration of 1×10^8–2×10^9 particles/mL. The samples were loaded to the sample chamber in a continuous flow by a syringe pump. The instrument was equipped with a 488 nm laser and a sCMOS camera. The focus for each sample was manually adjusted to achieve optimal visualization of particles and for each measurement, five videos of 60 s were captured. For all experiments the following settings were used: temperature: 25 °C; Syringe speed: 20; Viscosity: 0.9 cP; camera level setting ranged from 13 to 14 in light scatter mode (LSM). After capture, the videos have been analyzed by the in-build NanoSight Software NTA 3.4 Build 3.4.4 with a detection threshold of 5. The current study is documented and registered in EV-TRACK platform [30] with ID (EV240157).

2.6. Peripheral blood mononuclear cell treatments

HD-PBMCs (25×10^4/mL) were cultured with CM, EV-depleted CM (EVDCM), and EV-depleted medium (EVDM) for 30 min and 24 h. Furthermore, 1.25×10^5 PBMCs were exposed to 50 μg/mL of the sEVs and lEVs in accordance with a previous study [31], and 1 μg/mL [32] of Lipopolysaccharide (LPS) (CAT-L-2880, SIGMA®) (Darmstadt, Germany). EVs from FBS, diluted CM, EVDM and LPS were used as control experiments.

2.7. Western blotting

PBMC lysate was extracted with RIPA (Radioimmunoassayprecipitation Assay) lysis buffer and resolved using SDS-PAGE gel. Proteins were transferred onto polyvinylidene fluoride membranes and blocked with PBS with 0.1 % Tween 20 containing 5 % skim milk. Primary antibodies (Abs) against polyubiquitin chains (1:10000) (Clone P4D1, Santa Cruz), CD63 (1:10000) (SICGEN, Portugal), and Alix (1:2000) (SICGEN, Portugal) were used, followed by HRP-conjugated secondary Ab goat anti-mouse (1:10000), donkey anti-goat (1:10000). Immunoreactivity was analyzed using the ChemiDoc Touch System, and images were quantified with ImageJ software (version 1.53a).

2.8. Statistical analysis of Western blot data

Data analysis and visualization were performed using R Studio (2022.07.1), with experiments conducted at least in triplicates. Statistical comparisons between groups were conducted using two-tailed Student's *t*-Test. Statistical significance was defined as an adjusted *p*-value or p-value < 0.05.

2.9. Proteomics analysis

2.9.1. Peptide sample preparation

Samples containing a minimum of 20 μg of total proteins of whole-cell lysates or EVs were further processed by the filter-aided sample preparation method. In short, protein solutions containing SDS and DTT were loaded onto filtering columns (Millipore, Billerica, MA, USA) and washed exhaustively with 8 M urea in HEPES buffer [33,34]. Proteins were reduced with DTT and alkylated with IAA. Protein digestion was performed by overnight digestion with trypsin sequencing grade (Promega, Madison, WI, USA).

2.9.2. Mass spectrometry analysis

Peptide samples were analyzed by nano-liquid chromatography−mass spectrometry/ mass spectrometry (LC-MS/MS) (Dionex RSLCnano3000) coupled to an Exploris 480 Orbitrap mass spectrometer (Thermo Scientific) as previously described [35].

2.9.3. Coefficient of variation of replicas

In our proteomics profiling, we meticulously evaluated the precision of our experimental measurements, as evidenced by a calculated coefficient of variation of 24.6 %. This indicative measure underscores the reliability and consistency of protein abundance quantification across technical replicates, affirming the robustness of our proteomic profiling methodology.

2.9.4. MS database search

Raw LC-MS runs were analyzed using MaxQuant Version 2.1.0.05 [36]. A standard human proteome database from UniProt (3AUP000005640) with permutated protein sequences, where Arg and Lys were not permutated, was included in the database for database dependent search. A maximum of four missed trypsin cleavages were allowed for the search. Carbamidomethyl cysteine was specified as the fixed modification. Variable modifications included methionine oxidation, N-terminal protein acetylation, di-glycine tag, lysine acetylation, serine, threonine, and tyrosine phosphorylation. All other parameters for MaxQuant were default parameters. For VEMS the specific accuracy for precursor ions was 5 ppm mass accuracy and 0.01 *m/z* for fragment ions. A false discovery rate of 1 % for peptide and protein identification was applied. After confirming similar results by VEMS and MaxQuant subsequent statistical and functional analysis reported in this manuscript was based on the results from MaxQuant Version 2.1.0.05.

2.9.5. Quantitative analysis

The study involved a total of 20 subjects, each of whom was tested in two technical replicates, resulting in a total of 40 LC-MS measurements. Intensity-based absolute quantification [37] was estimated from total ion counts by dividing it by the number of theoretical canonical tryptic peptides for a given protein (missed cleavage theoretical peptides were not counted). R statistical programming language was used to analyze quantitative data from VEMS. We preprocessed the values of protein label-free expression by excluding common MS contaminants followed by $\log_2(x + 1)$ transformation, and quantile normalization. In the "limma" R package [38], we performed statistical analysis of quantitative values, focusing on the contrast between the proteome of immune cells in buffy coat samples from DLBCL patients and those from HDs. Multiple testing was corrected by applying the Benjamini and Hochberg methods [39]. We used ggplot2 to generate the Volcano plots. MS

quantified 913 proteins reliably (Supplementary Table S1 and B).

2.9.6. Functional enrichment analysis

Hypergeometric probability test according to the previous publications [40,41] was used for global functional enrichment analysis in R. Follow-up analysis was performed using DAVID [42], Reactome [43], STRING and ClueGO application (version 2.5.10) [44] in Cytoscape. Significantly up- and downregulated proteins (based on the p-value < 0.05) were all subjected to global functional enrichment analysis followed by detailed analysis using the annotations such as cellular component (CC), biological process (BP), molecular function (MF), KEGG pathway [45], Reactome [43] and proteostasis factors [46].

3. Results

3.1. Study overview and patients

PICs were collected from both DLBCL patients and HDs and each sample was analyzed twice by MS (Fig. 1, top panel and Table 1). The cancer cohort comprised 10 DLBCL patients, 5 diagnosed with non-GCB and 5 with GCB DLBCL (Table 2). None of the clinical parameters displayed a statistical association with non-GCB and GCB classification (Table 2). Functional enrichment analysis was performed on MS identified and differential regulated proteins. Subsequently, PBMCs from HDs were isolated, and SFs (corresponding to non-EV component), sEVs and lEVs were fractionated from CM of a DLBCL cell line using serial centrifugation (Fig. 1, bottom panel). The isolated PBMCs were treated with LPS, FBS EVs, EVDM, EVDCM, sEVs and lEVs, and the polyubiquitination levels were monitored using immunoblotting assays and cell viability estimated by trypan blue exclusion assay. Finally, the sEVs were subjected to further proteomics analysis using MS.

3.2. Proteomics profiling of peripheral immune cells separates patients with DLBCL from HDs

A principal component analysis (PCA) of quantitative data from all identified and quantified proteins obtained from an MS-based proteomic experiment without any data filtering, resulted in a clear separation between DLBCL and HDs along the first principal component (Fig. 2A, B). The analysis was conducted using the complete set of quantitative MS data without any prefiltering, making it an unsupervised approach. This contrasts with analyses that first extract regulated proteins before performing PCA. The obtained clear distinction underscores the robust discriminatory power of the proteomic data, suggesting substantial differences in the protein profiles between PICs isolated from patients with DLBCL and those from HDs. The PCA plots also indicate that there is more variance among DLBCL patients than HDs (Fig. 2A, B). Volcano plot based on limma statistical comparison of DLBCL and HDs confirmed a high number of statistically significant regulated proteins after correction for multiple testing (Fig. 2C). For this comparison, 135/205 (adjusted p-value < 0.05/p-value < 0.05) of the identified proteins were found downregulated in DLBCL compared to HD, with a $\log_2$ fold change range of regulation from -5.8 to -0.64. The number of upregulated proteins were 51/81 (adjusted p-value < 0.05/p-value < 0.05) and $\log_2$ fold change ranged from 0.62 to 3.28 for up regulated proteins (Supplementary Table S1). The heatmap in Fig. 2D indicates the z-score normalized expression values for 19 proteins with a least four-fold differential regulation and significant p-value after correction for multiple testing.

3.3. Functional enrichment analysis of differentially expressed proteins in DLBCL vs HDs

First, a global functional enrichment analysis was performed across multiple functional annotations to identify the most relevant databases [40,41]. Fig. 3A displays from top to bottom the top five significantly enriched functional entities in polyubiquitinated proteins, GO-BP, GO-

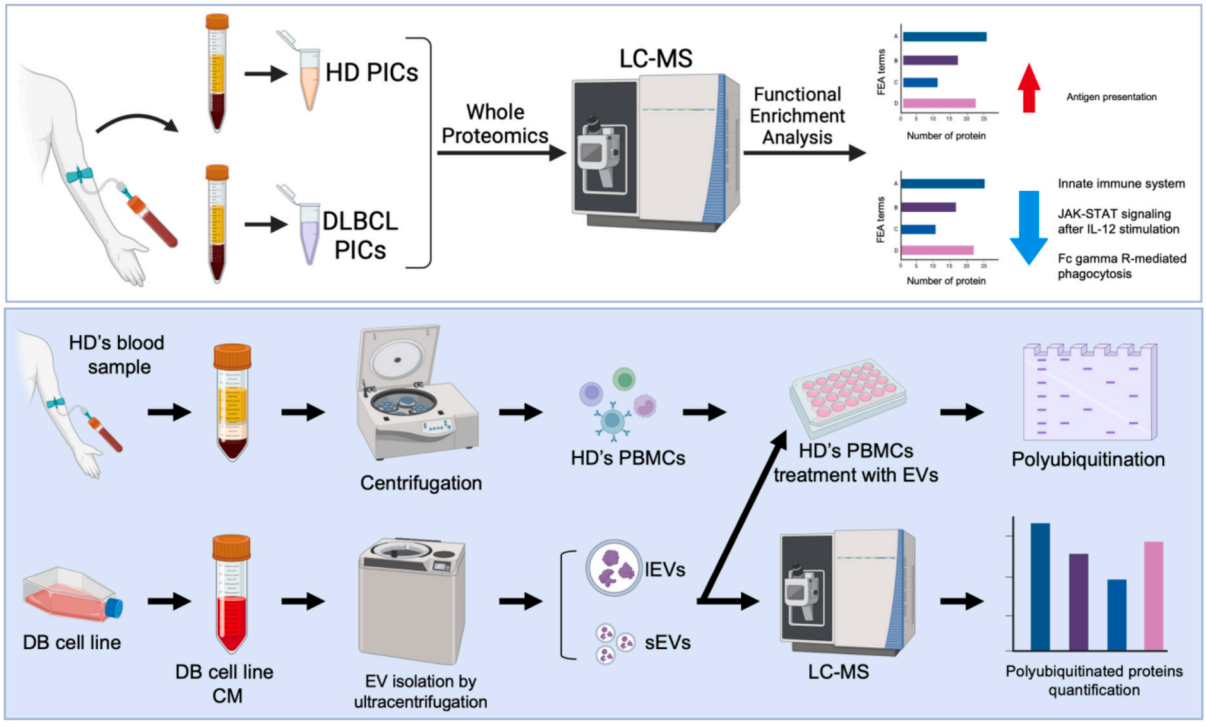

Fig. 1. General overview of the experimental workflow used in the study. Upper panel indicates the experimental workflow for patient-derived buffy coat-derived immune cell proteome profiling. Lower panel indicates experimental workflow elucidating the functional effects of SFs, sEVs, and lEVs on PBMCs from healthy donor. FEA: Functional enrichment analysis.

MF, GO-CC, KEGG pathways, and Reactome, respectively. The enriched functional categories are mainly associated with immune-related functions and proteins previously identified in tandem ubiquitin binding entities (TUBEs) enriched fractions [46]. The Reactome database provided the most comprehensive annotation of immune-related pathways. Consequently, the subsequent analysis focused on these immune-related pathways using the Reactome database and its analysis tools (Fig. 3B, C) and UPS-related pathways. A comparison of the enriched functional categories by the different software tools revealed high similarity with the main differences in the reported *p*-values, which can likely be explained by different corrections for multiple testing. The network analysis in Fig. 3B shows that the innate immune system constitutes the main component of the enriched proteins annotated as immune system-related. Follow-up analysis using Reactome software tools and databases revealed multiple immune system-related entities (Fig. 3C). Detailed analysis revealed that overall, the functions related to the innate immune system were mainly enriched in proteins that were downregulated between DLBCL and HDs. We further cross-checked specific regulations in innate immune system functions. This analysis revealed that nearly all proteins in the 'JAK-STAT signaling after interleukin-12 (IL-12) stimulation' and 'Fcγ receptor-dependent phagocytosis' pathways were downregulated, with 13 out of 15 and 15 out of 16 proteins downregulated, respectively. From the adaptive immune system, 'Antigen processing and presentation class I MHC' were moderately significantly enriched with 5 out of seven proteins upregulated. Given the significant enrichment in proteins previously reported as polyubiquitinated based on TUBE enrichment, all significant functional entities related to proteostasis related function across multiple databases were summarized in Fig. 3D and Supplementary Table S1C.

Overall, our data demonstrate that the proteome in the peripheral immune system of DLBCL patients was significantly affected by DLBCL and that UPS system may play a significant role.

3.4. PBMCs exposed to CM and EV-depleted CM accumulate polyubiquitin

Assuming that DLBCL tumor cells secretome can affect PICs, we have investigated the effect of DB cell line secretome on PBMCs from HDs. Firstly, PBMCs from HDs were cultured in 1:1 dilution of the DB-CM and medium and undiluted CM for 24 h using cell viability (Fig. 4A) and polyubiquitination western blots (Fig. 4B–C) as readouts. CM after 24 h is still nutrient sufficient, and the effect therefore cannot be explained by

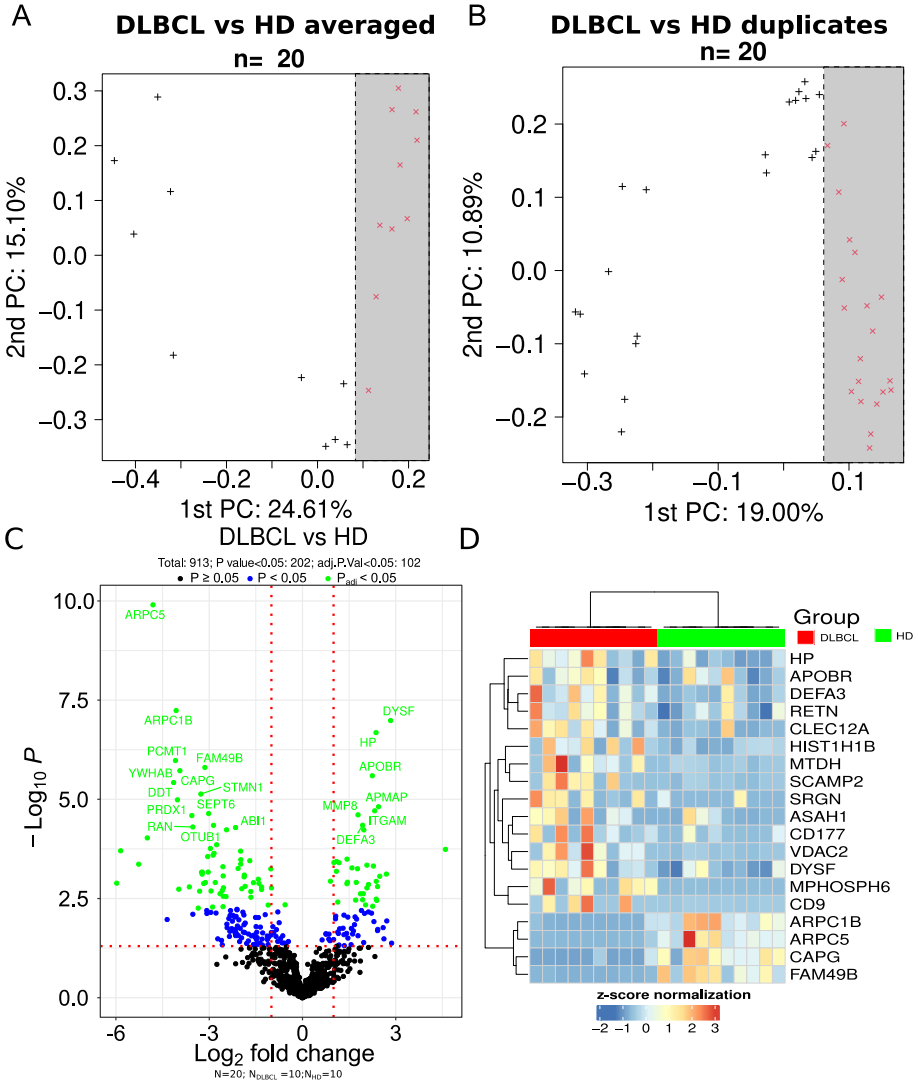

Fig. 2. Statistical comparison of proteins from PICs of DLBCL versus HD. A) PCA plot of averaged of duplicate LC-MS runs of all quantitative MS data without any pre-filtering and B) without averaging. C) Volcano plot for the comparison of DLBCL versus HD. The red horizontal line indicates a 0.05 p-value threshold. Red vertical lines indicate two-fold differential regulation. The number of regulated proteins indicated in the titles is based on *p*-values and adjusted p-values with an effect size greater than twofold. D) Heatmap of z-score normalized expression values of the top regulated proteins between DLBCL and HD.

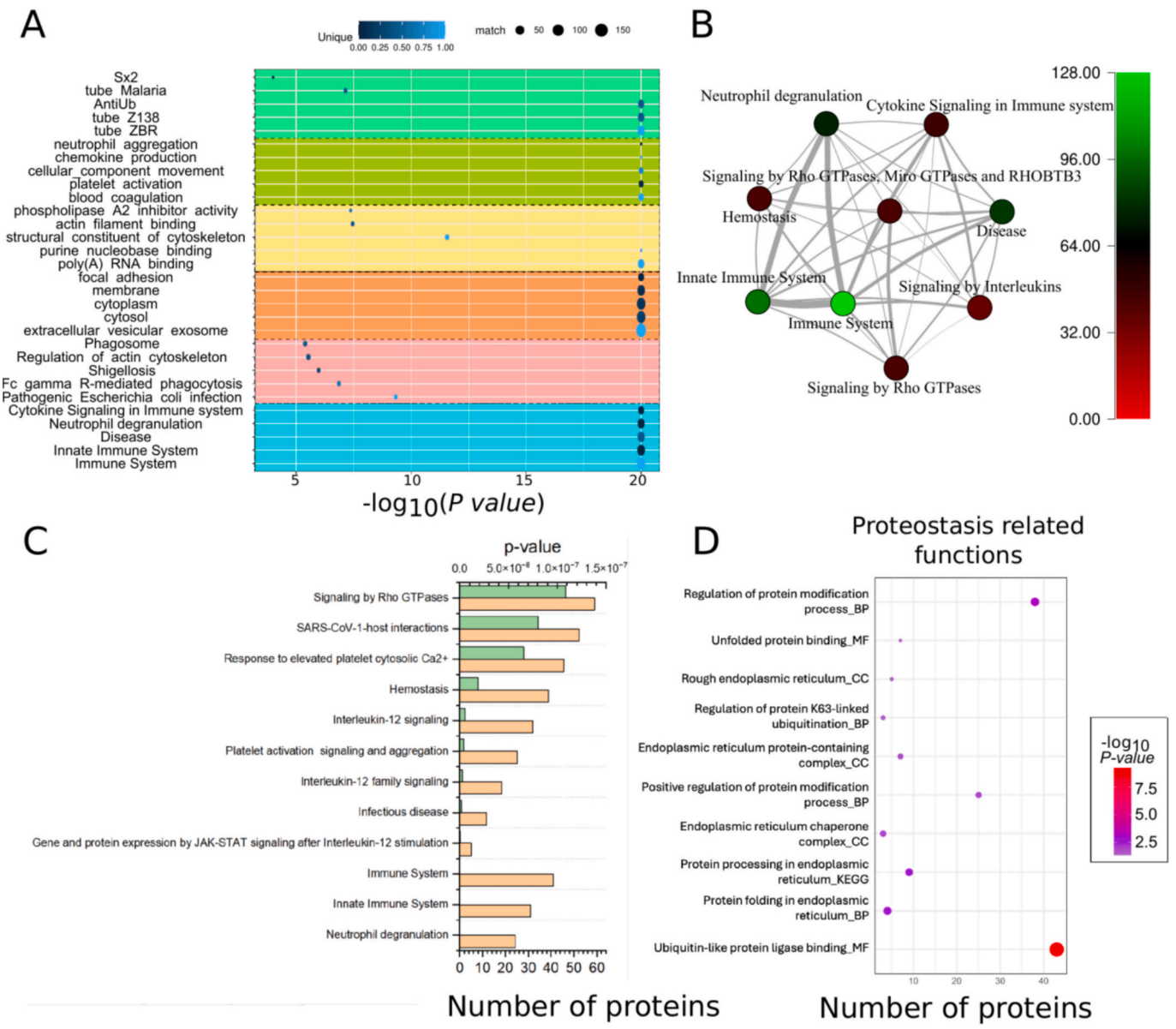

Fig. 3. Functional enrichment analysis of differentially regulated proteins between DLBCL and HD. A) Top five enriched functional categories identified across polyubiquitinated proteins, BP, MF, CC, KEGG pathways, and Reactome (from top to bottom). Dot color indicates uniqueness of the functional in comparison to functional terms with more significant enrichment. The size of the dots indicates the number of proteins significantly regulated matching the functional term. B) Network analysis of top Reactome enriched functional categories. Node color indicates number of proteins in the categories and edge thickness the overlap in proteins between entities. C) Detailed analysis of Reactome pathways. Green bars are associated to the *p*-value of enrichment and orange bar to number of matching proteins. D) All significant enriched UPS-related functions across GO-CC, GO-BP and GO-MF.

starvation. For instance, PBMCs that are cultured for 48 h without media exchanges exhibit no appreciable decline in cell viability (data not shown). To further control for starvation, 1:1 dilution experiment of CM and fresh medium were also performed to look for additive effects caused by CM. After 24 h of incubation, the number of cells in DB-CM showed a DB-CM concentration-dependent decrease in cell viability compared to control PBMCs by trypan blue exclusion assay (Fig. 4A). Undiluted CM resulted in a significant decrease in cell viability compared to control medium. Polyubiquitination was increased in a DB-CM concentration-dependent manner (Fig. 4B–C). Again, undiluted CM resulted in a significant increase in polyubiquitination.

To further address whether the DLBCL tumor secretome can affect the peripheral immune system, PBMCs from HDs were cultured with EVDCM from a DB cell line and EVDM using polyubiquitination western blots, and cell viability as readouts (Fig. 4D–E and F). It should be noted that despite ubiquitin's multiple roles in immune cells, polyubiquitination levels are much lower in PBMCs than in cancer cells (Fig. 4G). Consistent with previous findings, our western blot analysis of immune cells revealed low polyubiquitination signals compared to cancer cells, underscoring the concordance between our results and those reported in other studies [47]. Furthermore, polyubiquitinated protein levels were assessed in DB cell line-derived sEVs, lEVs, and EVDCM. PBMC analysis revealed variations in polyubiquitinated protein levels among sEVs, lEVs, and EVDCM exposures. After 30 min, no significant differences in cell viability were observed between EVDCM and EVDM (Fig. 4F). However, EVDCM displayed an increasing trend in polyubiquitination after 24 h (Fig. 4D–E) and a decreasing trend in cell viability after 24 h (Fig. 4F).

In summary, our results indicate that DB-CM decreased the viability of PBMCs and enhanced the levels of polyubiquitinated proteins within

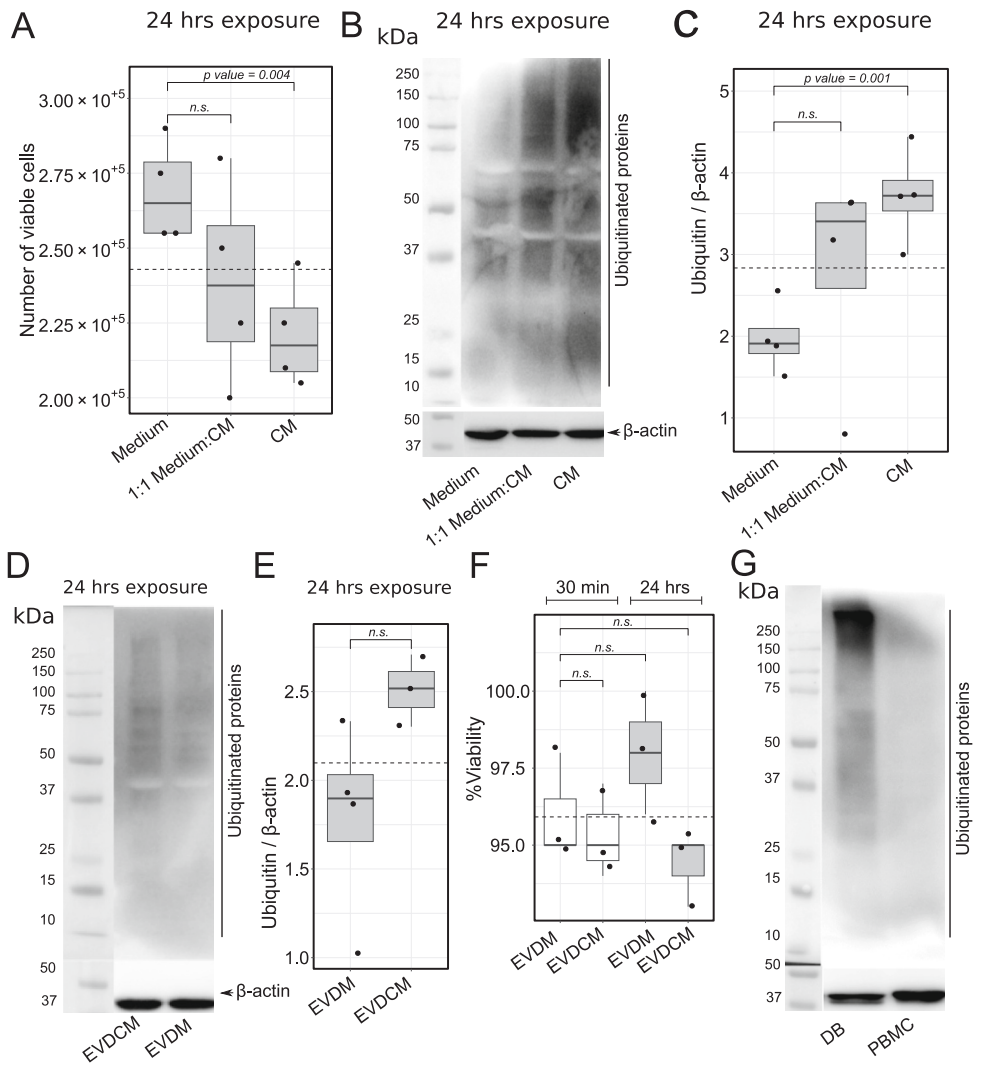

Fig. 4. PBMCs exposed to CM from DB cell line for 30 min (white boxes) and 24 h (grey boxes). A) Viability of PBMCs cultured in RPMI-1640 complete medium, diluted CM (1:1 diluted with fresh complete medium), and undiluted CM after 24 h. B) Western blot to evaluate the level of the polyubiquitinated proteins in PBMCs exposed to CM from DB cell line for 24 h. C) Quantification of ubiquitin levels in PBMCs based on western blots. D, E) Quantification of the western blot resulted from culturing PBMCs in EVDCM and EVDM. F) Viability of the PBMCs cultured in EVDM and EVDCM for 30 min and 24 h. G) Polyubiquitinated protein levels in DB versus PBMCs each lane was loaded with 30 μg total protein. CM: Conditioned Medium, PBMC: peripheral blood mononuclear cell. Dashed lines in boxplots represent the overall mean. hrs: hours.

PBMCs. DB-CM exhibited a more pronounced effect than EVDCM in inducing polyubiquitin increases (Fig. 4C vs E). Furthermore, DB-CM exposure was associated with significantly lower cell viability compared to EVDCM at 24 hour post-treatment (Fig. 4A vs F). Notably, this finding implied that the primary effect of CM was not mediated by small SFs, prompting us to investigate the role of EVs isolated from DB-CM in eliciting this response. This difference between DB-CM and EVDCM further suggests that our readouts are not due to starvation, as EVDCM would be expected to elicit the strongest response in that case.

3.5. EVs isolated from DB tumor cell line

sEVs and lEVs were isolated from the DB tumor cell line using differential centrifugation for subsequent in vitro functional analysis, as detailed in the following section. The in vitro isolated sEVs and lEVs were characterized by NTA (Supplementary Table S1D). sEVs isolation demonstrated an expected peak around 100 nm (Fig. 5A) and the particle size distribution for lEVs were broader and shifted to larger sizes (Fig. 5B). Transmission electron microscopy of sEVs and lEVs confirmed that majority of particles were around 100 nm (Fig. 5C–D). Western blotting for EV markers Alix indicated a clear enrichment of Alix in sEVs and low presence in lEVs (Fig. 5E). CD63 was present in both raw cell extract as well as in sEV and lEVs (Fig. 5F). Interestingly the sEVs showed highest level of polyubiquitin based on Western blot analysis of the same amount of protein input (Fig. 5G). Finally, sEVs were characterized based on MS data (Supplementary Table S1E), confirming identification of EV markers by EVqualityMS tool (https://github.com/ruma1974/EVqualityMS/tree/master) [48]. In total 2892 EV proteins were identified by LC-MS (Supplementary Table S1E). In conclusion, the isolated sEVs and lEVs displayed characterizations in line with previous studies [49,50] and therefore suitable for the subsequent functional study.

3.6. DB-derived EVs induce polyubiquitinated proteins in the PBMCs in a time-dependent manner

DB-CM was fractionated into sEVs and lEVs, which were then used to expose PBMCs from HDs. Again, polyubiquitination expression and cell viability were used as readout and short (30 min) and long incubation times (24 h) were investigated (see also method section PBMCs

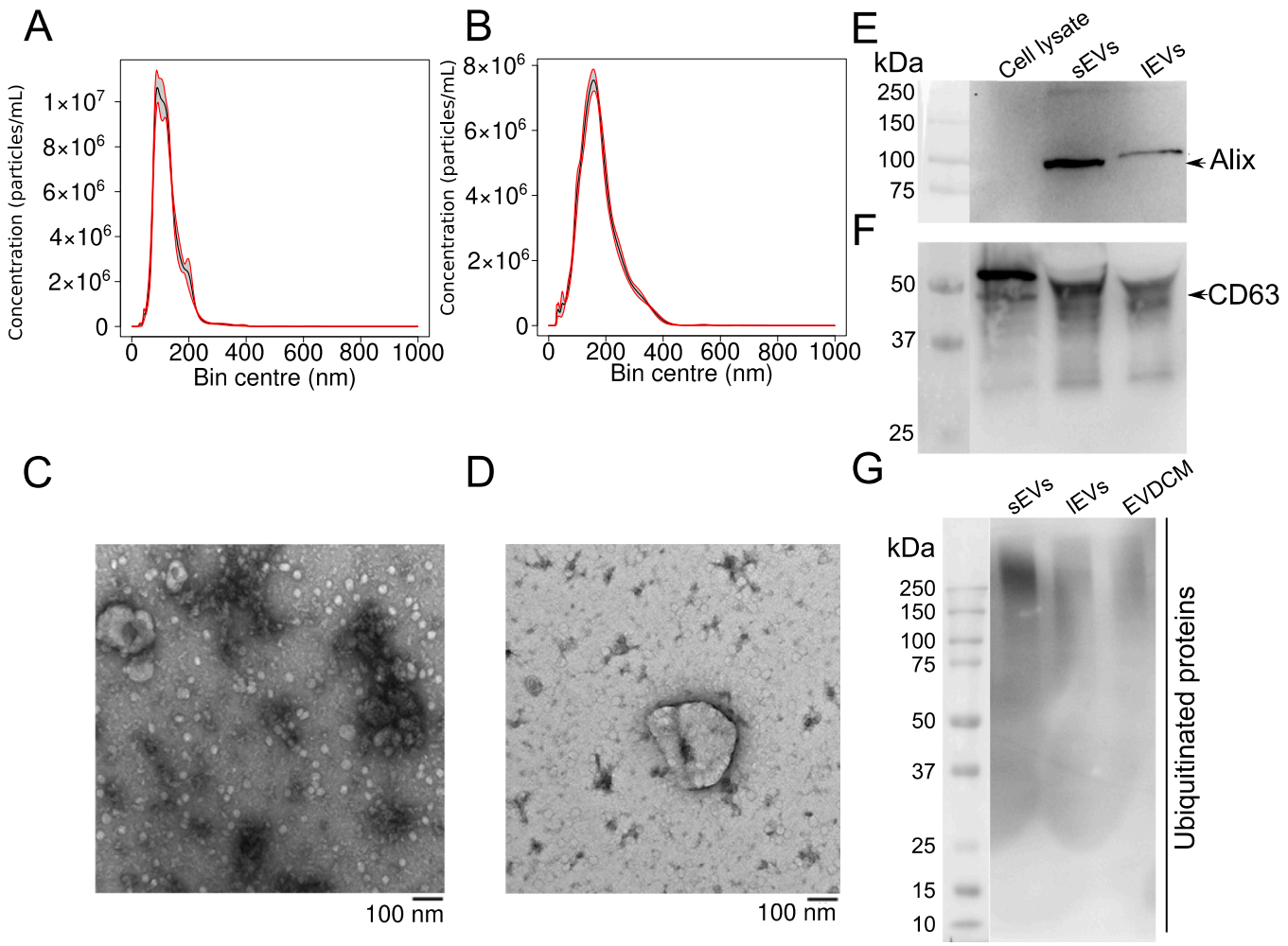

Fig. 5. Characterization of sEVs and lEVs. NTA conducted on representative samples of A) sEVs and B) lEVs. TEM image of DB C) sEVs and D) lEVs. Representative immunoblotting assay performed on DB cell lysate, sEVs and lEVs samples to detect E) Alix, F) CD63 and G) polyubiquitination.

treatments) (Fig. 6A, B). It's essential to note that the EVs (sEVs and lEVs) used in this study were concentrated through ultracentrifugation pelleting and then added to media at a concentrated level. Therefore, the observed effects cannot be attributed to media nutrient dilution. Additionally, control experiments with isolated FBS-EVs did not result in significant changes in readout parameters (Fig. 6C).

Following 30 min of treatment with DB-derived sEVs, PBMCs showed no significant changes in the number of viable cells (Fig. 6C, upper panel), while polyubiquitination levels exhibited a non-significant trend toward elevation (Fig. 6A, B). After 24 h of sEV exposure, a decreasing trend in PBMCs' viability (Fig. 6C, lower panel) and a significant increase in polyubiquitination were observed (Fig. 6A, B). We observed high level of polyubiquitinylation in sEVs (Fig. 5F). However, before western blot and proteome analysis by MS the cells are washed and additionally polyubiquitination is mainly observed on 24 hour exposure. Therefore, the increased polyubiquitination in PBMCs are either caused by absorbed polyubiquitinated EV proteins, or by an internal dysregulation of UPS machinery.

Exposure of PBMCs with lEVs displayed no significant changes in cell viability after 30 min (Fig. 6C, upper panel) but a significant increase in polyubiquitination (Fig. 6A, B). However, after 24 h of lEV exposure, cell viability decreased significantly, while polyubiquitination showed a marginally significant increase.

Finally, exposure to 1 μg LPS at 30 min and 24 h showed a similar effect as the sEV and lEV on PBMC viability (Fig. 6C).

Our data indicate that the treatment effect of tumor sEV and lEV are time-dependent and overall display a similar effect on immune cell viability as LPS. Significant changes in polyubiquitin levels were observed earlier than significant changes in cell viability. lEV appeared to have the strongest effect on cell viability compared to sEV and lEVs resulted in a faster increase in polyubiquitin compared to sEVs.

4. Discussion

Our study identified differences in the PICs proteome between DLBCL and HD subjects (Fig. 2, Supplementary Table S1A). Currently, blood cell population analysis lacks conclusive prognostic value for DLBCL [51]. Although bone marrow involvement can occur, detecting tumor cells in the peripheral blood is often below diagnostic levels. However, circulating tumor DNA has shown potential as a biomarker [52]. Our results highlight significant alterations in the PIC proteome in DLBCL, prompting us to perform functional enrichment analysis. Functional enrichment analysis of differentially regulated proteins (p-value < 0.05) revealed that among KEGG and Reactome pathways the immune system, the innate immune system and cytokine signaling in immune system were overrepresented pathways (Fig. 3). Key pathways such as Fc-γ receptor-dependent phagocytosis and neutrophil degranulation were notably affected within the innate immune system, while gene and protein expression by JAK-STAT signaling after IL-12 stimulation was represented within the cytokine signaling pathways (Fig. S1A). Fc-γ receptor-dependent phagocytosis pathway is downregulated in white blood cells of DLBCL patients (Fig. S1B). The proteome analysis revealed

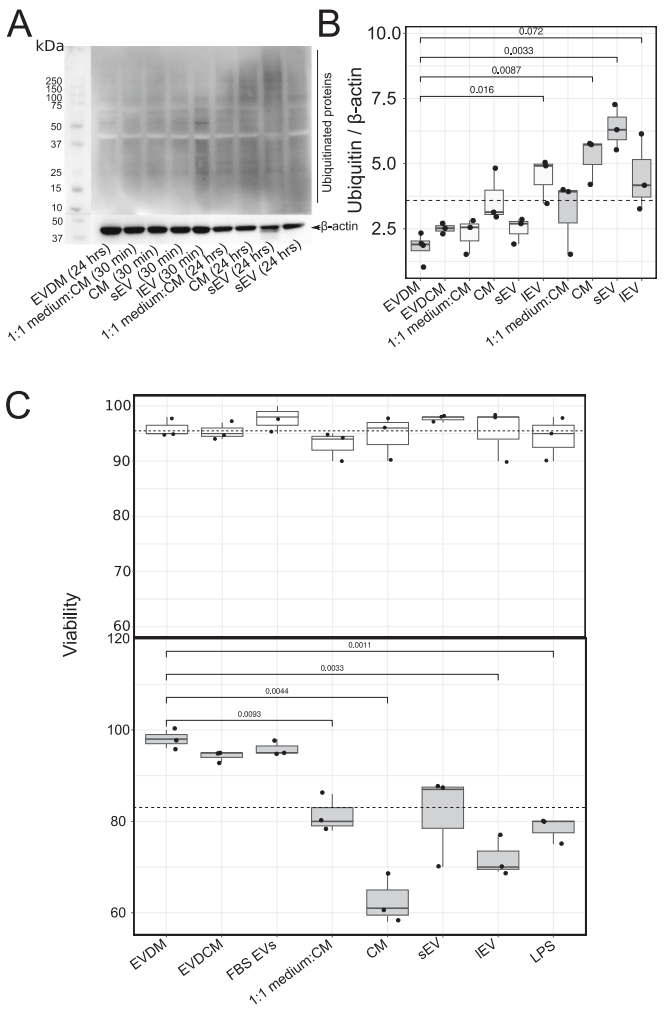

Fig. 6. PBMCs exposed to EVDM, EVDCM, CM, sEV, and lEVs derived from DB cell line for 30 min (white boxes) and 24 h (grey boxes). A, B) Immunoblot assays of the polyubiquitinated protein levels in PBMCs after different exposure times. C) Viability assay after various exposures of 30 min (white boxes upper panel) and 24 h (grey boxes lower panel). CM: Conditioned Medium, PBMC: peripheral blood mononuclear cell, diluted CM: 1:1 diluted CM with fresh complete medium. Cells were exposed to 50 μg EVs and 1 μg LPS.

that DLBCL PICs were enriched for activated neutrophils markers like CD177 and MPO [53], aligning with previous findings that neutrophils play a major role in the inflammatory response in DLBCL, and the neutrophil-to-lymphocyte ratio holds prognostic value [54]. Fcγ receptors have activating or inhibitory functions and are expressed by various immune cells in combination that depend on the specific cell type [55]. In neutrophils, Fcγ receptor expression can be upregulated upon inflammatory cytokines stimulus. Since we observed down-regulation of this pathway our results suggests that downstream pathway signaling maybe compromised leading to an immune suppressive environment at a systemic level in DLBCL. The tumor interference with hematopoiesis unbalances the cytokine profiles interfering with the signaling pathways which consequently could alter Fcγ receptor expression [56].

Given the low abundance of DLBCL tumor cells in peripheral blood and the strong dysregulation of the immunoproteome observed in our study, a combination of extracellular soluble mediators, EVs, and non-EV nanoparticles likely mediates intracellular communication [57]. Previously the proteome of plasma EVs of the DLBCL patients and HD was characterized, revealing that EV proteome is strongly affected by DLBCL status, in turn suggesting that a differential population of EVs can modulate the patient's immune response [24,33]. Particularly, we have identified alterations in the expression of immunoglobulins which may regulate the availability of Fcγ receptor ligands. We hypothesize that Fcγ receptor-mediated phagocytosis in DLBCL can be signaled through the UPS as previously reported to be important in cells of myeloid origin [58]. Internalization of antibody-associated antigens involves the activation of NF-κB and MAPK signaling via substrate ubiquitylation [59]. Alternatively, the phagocytic pathway could regulate Fcγ receptor expression, and the receptor is either degraded or recycled. Fcγ receptor phagocytosis may undergo a series of events in which the phagosome maturation includes several fusions within the endocytic pathway. Both ubiquitylated proteins and the proteasome function are involved in the formation of multivesicular structures, likely dictating the fate of Fcγ receptor into the phagolysosome, to endocytic vesicles to recycling to the plasma membrane or to the multivesicular compartment [60]. Concomitantly, ARPC5 is downregulated ($\log_2FC = -4.6$, adjusted p-value $= 2 \times 10^{-11}$) in DLBCL PICs proteome, which is ubiquitinylated by 'Gene related to anergy in lymphocytes' protein (GRAIL) with Lys-63-linked chains, leading to proteasomal degradation [61]. ARPC5 belongs to the Arp2/3 complex required for actin nucleation and actin filament polymerization in diverse critical cellular functions including phagocytosis, vesicular trafficking and lamellipodia extension, suggesting that ubiquitination can be involved in the downstream signaling of Fcγ receptor-dependent phagocytosis pathway. Among the identified terms from functional enrichment analysis for comparison of the PICs' proteome from DLBCL patients versus HDs several protein hemostasis-related functions, particularly UPS-related terms, were identified (Fig. 3D). These functions contained both up and downregulated proteins. Polyubiquitination plays a regulatory role in various signaling pathways known for their diverse roles in activating and regulating immune cells' functions [62,63]. The effects of DLBCL cells and their secretome on polyubiquitination in PICs have been relatively unexplored in DLBCL. However, several reports showed that EVs derived from non-malignant and malignant cells can affect UPS in recipient cells. For instance, Liao, H.X. et al. [64] showed that exosomes released by non-malignant cells like mesenchymal stem cells alter immune cells' signaling pathways and immune cell activation through changes in ubiquitination. Additionally, it has been demonstrated that exosomes released by cancer cells contain E3 ubiquitin ligase like TRIM59 which could be transferred to immune cells. TRIM59 interacts with ABHD5 and increases the ubiquitination and proteasome degradation which leads to metabolic reprogramming and induces NLRP3 inflammasome activation in immune cells [65]. In alignment with previous literature our study adds the observation of significant dysregulation of UPS-factors in PICs between DLBCL and HD subjects (Supplementary Table S1C). Building on this knowledge, we aimed at investigating how tumor EVs affects polyubiquitination in PBMCs. The polyubiquitination signaling cascade can be triggered by EVs, as EV exposure to PBMCs resulted in an increase in cellular polyubiquitination. This effect was more pronounced for the sEVs compared to lEVs in a longer exposure time. To further elucidate the underlying causes of this UPS dysfunction caused by EVs, future studies are warranted to investigate whether the observed effect is primarily driven by alterations in proteasome activity and/or deubiquitinase function. Specifically, it would be valuable to explore the relationship between decreased proteasome activity, deubiquitinating enzyme activity, and increased polyubiquitination ligase activity. Resolving these questions could provide further critical clues regarding the molecular mechanisms underlying UPS dysregulation in DLBCL. On the other hand, differently regulated proteins from the comparison of PICs of the DLBCL patients versus HDs were also enriched for IL family pathways, particularly IL-12 and IL-4/13 mediated stimulation (Fig. 6). sEVs and lEV exhibited overlapping size distributions (Fig. 5A, B), shared detectable EV markers (CD), and produced comparable functional effects on PBMCs (Fig. 6B, C). However, the quantitative level of the EV markers differed significantly between sEV and lEVs and significant functional difference was observed in their temporal profile

(Fig. 6B, C). It will be essential in the future to develop more accurate EV separation methodology to improve understanding of EV sub population function. In addition, future research needs to address precisely which molecules on EVs are responsible for the observed effects on peripheral immune cell proteome in our in vitro model system. For the peripheral immune cell proteome changes observed in patients, the question becomes inherently more complex since EVs from TME possibly bind proteins from other cells in the TME which possibly are shuttled to the peripheral system with potential effects on peripheral immune cells proteome.

As mentioned above DLBCL might induce immune suppression. Our data highlight a potential role of the IL-12 signaling network in DLBCL-associated immunosuppression. Dysregulation of gene and protein expression via JAK-STAT signaling following IL-12 stimulation may impair Th1 cell differentiation. Since Th1 cells recruit cytotoxic NK cells and $CD8^+$ T cells, which mediate anti-tumor activity [66], this disruption could contribute to the observed immune downregulation in this study.

5. Conclusion

In conclusion, this study reveals a dysregulated immune system response such as downregulation of 'JAK-STAT signaling after IL-12 stimulation' and 'Fcγ receptor-dependent phagocytosis' pathways in cells isolated from buffy coat samples of the treatment naive DLBCL patients. Follow-up, in vitro experiments showed that mainly DB-CM-derived sEVs, and lEVs induced polyubiquitination and decrease in cell viability in PBMCs, demonstrating the potential of DLBCL-derived EV affecting peripheral immune system. Notwithstanding the limited sample size, our findings suggest a potential utility for proteome analysis of PICs in monitoring and diagnosing DLBCL, as significant differences were observed between immune cells isolated from HDs and those from DLBCL patient buffy coat samples. Given the relative ease of buffy coat cell isolation, it may be a more feasible and effective target for verification stage purposes than plasma-derived sEVs in distinguishing between DLBCL and Hodgkin lymphoma.

Supplementary data to this article can be found online at https://doi.org/10.1016/j.bbadis.2025.167842.

AI statement

During the preparation of this work the authors used ChatGpt in order to improve grammar of a few sentences. After using this tool, the authors reviewed and edited the content as needed and take full responsibility for the content of the publication.

CRediT authorship contribution statement

Mostafa Ejtehadifar: Writing – review & editing, Writing – original draft, Visualization, Validation, Methodology, Investigation, Formal analysis, Conceptualization. **Sara Zahedi:** Writing – review & editing, Methodology, Conceptualization. **Paula Gameiro:** Writing – review & editing, Resources, Methodology, Conceptualization. **José Cabeçadas:** Writing – review & editing, Methodology, Conceptualization. **Manuel S. Rodriguez:** Writing – review & editing, Methodology. **Maria Gomes da Silva:** Writing – review & editing, Resources, Methodology, Conceptualization. **Hans Christian Beck:** Writing – review & editing, Resources, Methodology, Investigation. **Rune Matthiesen:** Writing – review & editing, Writing – original draft, Visualization, Validation, Supervision, Resources, Project administration, Methodology, Investigation, Funding acquisition, Formal analysis, Conceptualization. **Ana Sofia Carvalho:** Writing – review & editing, Writing – original draft, Visualization, Validation, Supervision, Resources, Project administration, Methodology, Investigation, Funding acquisition, Formal analysis, Conceptualization.

Declaration of competing interest

The authors declare the following financial interests/personal relationships which may be considered as potential competing interests: Ana Sofia Carvalho and Rune Matthiesen reports financial support, article publishing charges, and equipment, drugs, or supplies were provided by Fundação para a Ciência e a Tecnologia. Rune Matthiesen reports financial support was provided by Horizon 2020. If there are other authors, they declare that they have no known competing financial interests or personal relationships that could have appeared to influence the work reported in this paper.

Acknowledgments

R.M. is supported by Fundação para a Ciência e a Tecnologia (CEEC position, DOI:10.54499/CEECIND/03906/2017/CP1421/CT0004). A. S.C. is supported by Fundação para a Ciência e a Tecnologia (DOI:10.54499/DL57/2016/CP1457/CT0013). This work is funded by FEDER funds through the COMPETE 2020 Programme and National Funds through FCT—Portuguese Foundation for Science and Technology under the projects number PTDC/BTM-TEC/1746/2021, PTDC/BTM-TEC/30087/2017 and PTDC/BTM-TEC/30088/2017. The project was supported by from European Union to advance EV research (Horizon2020_GA_n°101079264, EVCA and Horizon Europe-SE2023/GA101183034). We acknowledge the COST Action CA20113 "PROTEOCURE" supported by COST (European Cooperation in Science and Technology). This article is also a result of the projects (iNOVA4-Health–UIDB/04462/2020 and UIDP/04462/2020), and by the Associated Laboratory LS4FUTURE (LA/P/0087/2020), two programs financially supported by Fundação para a Ciência e a Tecnologia/Ministério da Ciência, Tecnologia e Ensino Superior. We thank Instituto Gulbenkian de Ciência for use of transmission electron microscopy.

Data availability

The MS proteomics data that support the findings of this study have been deposited in ProteomeXchange Consortium [67] via the PRIDE [68] partner with the PXD052494 accession code and project https://doi.org/10.6019/PXD052494.

References

[1] H. Huang, L. Fan, D. Fu, Q. Lin, J. Shen, Clinical characteristics and outcomes of patients with diffuse large B cell lymphoma treated with R-CHOP-like or CHOP-like regimens: an 8-year experience from a single center, Ann. Palliat. Med. 9 (2020) (1442452-1441452).
[2] C. Sarkozy, L.H. Sehn, Management of relapsed/refractory DLBCL, Best Pract. Res. Clin. Haematol. 31 (2018) 209–216.
[3] A.A. Alizadeh, M.B. Eisen, R.E. Davis, C. Ma, I.S. Lossos, A. Rosenwald, J. C. Boldrick, H. Sabet, T. Tran, X. Yu, Distinct types of diffuse large B-cell lymphoma identified by gene expression profiling, Nature 403 (2000) 503–511.
[4] M. Autio, S.-K. Leivonen, O. Brück, M.-L. Karjalainen-Lindsberg, T. Pellinen, S. Leppä, Clinical impact of immune cells and their spatial interactions in diffuse large B-cell lymphoma microenvironment, Clin. Cancer Res. 28 (2022) 781–792.
[5] D.W. Scott, R.D. Gascoyne, The tumour microenvironment in B cell lymphomas, Nat. Rev. Cancer 14 (2014) 517–534.
[6] T.F. Gajewski, H. Schreiber, Y.-X. Fu, Innate and adaptive immune cells in the tumor microenvironment, Nat. Immunol. 14 (2013) 1014–1022.
[7] E.J. Wherry, M. Kurachi, Molecular and cellular insights into T cell exhaustion, Nat. Rev. Immunol. 15 (2015) 486–499.
[8] E.J. Clappaert, A. Murgaski, H. Van Damme, M. Kiss, D. Laoui, Diamonds in the rough: harnessing tumor-associated myeloid cells for cancer therapy, Front. Immunol. 9 (2018) 2250.
[9] A.G. Solimando, T. Annese, R. Tamma, G. Ingravallo, E. Maiorano, A. Vacca, G. Specchia, D. Ribatti, New insights into diffuse large B-cell lymphoma pathobiology, Cancers 12 (2020) 1869.
[10] B. Manfroi, T. McKee, J.F. Mayol, S. Tabruyn, S. Moret, C. Villiers, C. Righini, M. Dyer, M. Callanan, P. Schneider, CXCL-8/IL8 produced by diffuse large B-cell lymphomas recruits neutrophils expressing a proliferation-inducing ligand APRIL, Cancer Res. 77 (2017) 1097–1107.
[11] T. Hirz, E.-L. Matera, K. Chettab, L.P. Jordheim, D. Mathé, A. Evesque, J. Esmenjaud, G. Salles, C. Dumontet, Neutrophils protect lymphoma cells against

cytotoxic and targeted therapies through CD11b/ICAM-1 binding, Oncotarget 8 (2017) 72818.
[12] F. Marchesi, M. Cirillo, A. Bianchi, M. Gately, O.M. Olimpieri, E. Cerchiara, D. Renzi, A. Micera, B.O. Balzamino, S. Bonini, High density of CD68+/CD163+ tumour-associated macrophages (M2-TAM) at diagnosis is significantly correlated to unfavorable prognostic factors and to poor clinical outcomes in patients with diffuse large B-cell lymphoma, Hematol. Oncol. 33 (2015) 110–112.
[13] M. Nie, L. Yang, X. Bi, Y. Wang, P. Sun, H. Yang, P. Liu, Z. Li, Y. Xia, W. Jiang, Neutrophil extracellular traps induced by IL8 promote diffuse large B-cell lymphoma progression via the TLR9 signaling, Clin. Cancer Res. 25 (2019) 1867–1879.
[14] C. Keane, D. Gill, F. Vari, D. Cross, L. Griffiths, M. Gandhi, CD4+ tumor infiltrating lymphocytes are prognostic and independent of R-IPI in patients with DLBCL receiving R-CHOP chemo-immunotherapy, Am. J. Hematol. 88 (2013) 273–276.
[15] M. Autio, S.-K. Leivonen, O. Brück, S. Mustjoki, J.M. Jørgensen, M.-L. Karjalainen-Lindsberg, K. Beiske, H. Holte, T. Pellinen, S. Leppä, Immune cell constitution in the tumor microenvironment predicts the outcome in diffuse large B-cell lymphoma, Haematologica 106 (2021) 718.
[16] Q.-C. Cai, H. Liao, S.-X. Lin, Y. Xia, X.-X. Wang, Y. Gao, Z.-X. Lin, J.-B. Lu, H.-Q. Huang, High expression of tumor-infiltrating macrophages correlates with poor prognosis in patients with diffuse large B-cell lymphoma, Med. Oncol. 29 (2012) 2317–2322.
[17] S. Riihijärvi, I. Fiskvik, M. Taskinen, H. Vajavaara, M. Tikkala, O. Yri, M.-L. Karjalainen-Lindsberg, J. Delabie, E. Smeland, H. Holte, Prognostic influence of macrophages in patients with diffuse large B-cell lymphoma: a correlative study from a Nordic phase II trial, Haematologica 100 (2015) 238.
[18] R. McCord, C.R. Bolen, H. Koeppen, E.E. Kadel III, M.Z. Oestergaard, T. Nielsen, L. H. Sehn, J.M. Venstrom, PD-L1 and tumor-associated macrophages in de novo DLBCL, Blood Adv. 3 (2019) 531–540.
[19] L. Li, R. Sun, Y. Miao, T. Tran, L. Adams, N. Roscoe, B. Xu, G.C. Manyam, X. Tan, H. Zhang, PD-1/PD-L1 expression and interaction by automated quantitative immunofluorescent analysis show adverse prognostic impact in patients with diffuse large B-cell lymphoma having T-cell infiltration: a study from the International DLBCL Consortium Program, Mod. Pathol. 32 (2019) 741–754.
[20] C. Jiménez-Cortegana, N. Palazón-Carrión, A.M. Garcia-Sancho, E. Nogales-Fernandez, F. Carnicero-González, E. Ríos-Herranz, F. de la Cruz-Vicente, G. Rodríguez-García, R. Fernández-Álvarez, A.R. Dominguez, Circulating myeloid-derived suppressor cells and regulatory T cells as immunological biomarkers in refractory/relapsed diffuse large B-cell lymphoma: translational results from the R2-GDP-GOTEL trial, J. Immunother. Cancer 9 (2021).
[21] W. Vermi, A. Micheletti, G. Finotti, C. Tecchio, F. Calzetti, S. Costa, M. Bugatti, S. Calza, C. Agostinelli, S. Pileri, Slan+ monocytes and macrophages mediate CD20-dependent b-cell lymphoma elimination via ADCC and ADCP, Cancer Res. 78 (2018) 3544–3559.
[22] S.S. McAllister, R.A. Weinberg, The tumour-induced systemic environment as a critical regulator of cancer progression and metastasis, Nat. Cell Biol. 16 (2014) 717–727.
[23] G. Andreola, L. Rivoltini, C. Castelli, V. Huber, P. Perego, P. Deho, P. Squarcina, P. Accornero, F. Lozupone, L. Lugini, A. Stringaro, A. Molinari, G. Arancia, M. Gentile, G. Parmiani, S. Fais, Induction of lymphocyte apoptosis by tumor cell secretion of FasL-bearing microvesicles, J. Exp. Med. 195 (2002) 1303–1316.
[24] R. Matthiesen, P. Gameiro, A. Henriques, C. Bodo, M.C.S. Moraes, B. Costa-Silva, J. Cabecadas, M. Gomes da Silva, H.C. Beck, A.S. Carvalho, Extracellular vesicles in diffuse large B cell lymphoma: characterization and diagnostic potential, Int. J. Mol. Sci. 23 (2022).
[25] A. Clayton, J.P. Mitchell, J. Court, M.D. Mason, Z. Tabi, Human tumor-derived exosomes selectively impair lymphocyte responses to interleukin-2, Cancer Res. 67 (2007) 7458–7466.
[26] K.H.W. Yim, A. Al Hrout, S. Borgoni, R. Chahwan, Extracellular vesicles orchestrate immune and tumor interaction networks, Cancers 12 (2020).
[27] E. Gargiulo, E. Viry, P.E. Morande, A. Largeot, S. Gonder, F. Xian, N. Ioannou, M. Benzarti, F.B. Kleine Borgmann, M. Mittelbronn, G. Dittmar, P.V. Nazarov, J. Meiser, B. Stamatopoulos, A.G. Ramsay, E. Moussay, J. Paggetti, Extracellular vesicle secretion by leukemia cells in vivo promotes CLL progression by hampering antitumor T-cell responses, Blood Cancer Discov. 4 (2023) 54–77.
[28] W. Liu, M. Zhu, H. Wang, W. Wang, Y. Lu, Diffuse large B cell lymphoma-derived extracellular vesicles educate macrophages to promote tumours progression by increasing PGC-1β, Scand. J. Immunol. 91 (2020) e12841.
[29] S.A. Bhat, Z. Vasi, R. Adhikari, A. Gudur, A. Ali, L. Jiang, R. Ferguson, D. Liang, S. Kuchay, Ubiquitin proteasome system in immune regulation and therapeutics, Curr. Opin. Pharmacol. 67 (2022) 102310.
[30] J. Van Deun, P. Mestdagh, P. Agostinis, Ö. Akay, S. Anand, J. Anckaert, Z. A. Martinez, T. Baetens, E. Beghein, L. Bertier, EV-TRACK: transparent reporting and centralizing knowledge in extracellular vesicle research, Nat. Methods 14 (2017) 228–232.
[31] A. Pando, C. Schorl, L.D. Fast, J.L. Reagan, Tumor derived extracellular vesicles modulate gene expression in T cells, Gene 850 (2023) 146920.
[32] K. Gärtner, C. Battke, J. Dünzkofer, C. Hüls, B. von Neubeck, M.K. Kellner, E. Fiestas, S. Fackler, S. Lang, R. Zeidler, Tumor-derived extracellular vesicles activate primary monocytes, Cancer Med. 7 (2018) 2013–2020.
[33] A.S. Carvalho, H. Baeta, A.F. Henriques, M. Ejtehadifar, E.M. Tranfield, A.L. Sousa, A. Farinho, B.C. Silva, J. Cabeçadas, P. Gameiro, Proteomic landscape of extracellular vesicles for diffuse large B-cell lymphoma subtyping, Int. J. Mol. Sci. 22 (2021) 11004.
[34] J.R. Wisniewski, A. Zougman, M. Mann, Combination of FASP and StageTip-based fractionation allows in-depth analysis of the hippocampal membrane proteome, J. Proteome Res. 8 (2009) 5674–5678.
[35] S. Ribeiro, A.R. Simoes, F. Rocha, I.S. Vala, A.T. Pinto, A. Ministro, E. Poli, I. M. Diegues, F. Pina, M.A. Benadjaoud, S. Flamant, R. Tamarat, H. Osorio, D. Pais, D. Casal, F.J. Pinto, R. Matthiesen, M. Fiuza, S. Constantino Rosa Santos, Molecular changes in cardiac tissue as a new marker to predict cardiac dysfunction induced by radiotherapy, Front. Oncol. 12 (2022) 945521.
[36] J. Cox, M. Mann, MaxQuant enables high peptide identification rates, individualized p.p.b.-range mass accuracies and proteome-wide protein quantification, Nat. Biotechnol. 26 (2008) 1367–1372.
[37] B. Schwanhausser, D. Busse, N. Li, G. Dittmar, J. Schuchhardt, J. Wolf, W. Chen, M. Selbach, Global quantification of mammalian gene expression control, Nature 473 (2011) 337–342.
[38] G.K. Smyth, Linear models and empirical bayes methods for assessing differential expression in microarray experiments, Stat. Appl. Genet. Mol. Biol. 3 (2004).
[39] Y. Benjamini, Y. Hochberg, Controlling the false discovery rate: a practical and powerful approach to multiple testing, J. R. Stat. Soc. B. Methodol. 57 (1995) 289–300.
[40] A.S. Carvalho, H. Molina, R. Matthiesen, New insights into functional regulation in MS-based drug profiling, Sci. Rep. 6 (2016) 18826.
[41] M. Hackenberg, R. Matthiesen, Annotation-modules: a tool for finding significant combinations of multisource annotations for gene lists, Bioinformatics 24 (2008) 1386–1393.
[42] B.T. Sherman, M. Hao, J. Qiu, X. Jiao, M.W. Baseler, H.C. Lane, T. Imamichi, W. Chang, DAVID: a web server for functional enrichment analysis and functional annotation of gene lists (2021 update), Nucleic Acids Res. 50 (2022) W216–W221.
[43] K. Rothfels, M. Milacic, L. Matthews, R. Haw, C. Sevilla, M. Gillespie, R. Stephan, C. Gong, E. Ragueneau, B. May, Using the reactome database, Curr. Protoc. 3 (2023) e722.
[44] G. Bindea, B. Mlecnik, H. Hackl, P. Charoentong, M. Tosolini, A. Kirilovsky, W.-H. Fridman, F. Pagès, Z. Trajanoski, J. Galon, ClueGO: a Cytoscape plug-in to decipher functionally grouped gene ontology and pathway annotation networks, Bioinformatics 25 (2009) 1091–1093.
[45] K.F. Aoki, M. Kanehisa, Using the KEGG database resource, Curr. Protoc. Bioinformatics 11 (2005) (1.12. 11–11.12. 54).
[46] F. Lopitz-Otsoa, E. Rodriguez-Suarez, F. Aillet, J. Casado-Vela, V. Lang, R. Matthiesen, F. Elortza, M.S. Rodriguez, Integrative analysis of the ubiquitin proteome isolated using Tandem Ubiquitin Binding Entities (TUBEs), J. Proteome 75 (2012) 2998–3014.
[47] J.-L.C. Mougeot, Z. Li, A.E. Price, F.A. Wright, B.R. Brooks, Microarray analysis of peripheral blood lymphocytes from ALS patients and the SAFE detection of the KEGG ALS pathway, BMC Med. Genet. 4 (2011) 1–19.
[48] R. Bernardino, A.S. Carvalho, M.J. Hall, L. Alves, R. Leão, R. Sayyid, H. Pereira, H. C. Beck, L.C. Pinheiro, R. Henrique, N. Fleshner, R. Matthiesen, Profiling of urinary extracellular vesicle protein signatures from patients with cribriform and intraductal prostate carcinoma in a cross-sectional study, Sci. Rep. 14 (1) (2024) 25065, https://doi.org/10.1038/s41598-024-75272-w. PMID: 39443544; PMCID: PMC11500006.
[49] A.S. Carvalho, M.C.S. Moraes, C. Hyun Na, I. Fierro-Monti, A. Henriques, S. Zahedi, C. Bodo, E.M. Tranfield, A.L. Sousa, A. Farinho, L.V. Rodrigues, P. Pinto, C. Barbara, L. Mota, T.T. Abreu, J. Semedo, S. Seixas, P. Kumar, B. Costa-Silva, A. Pandey, R. Matthiesen, Is the proteome of bronchoalveolar lavage extracellular vesicles a marker of advanced lung cancer? Cancers 12 (2020).
[50] F. Mantile, M. Kisovec, G. Adamo, D.P. Romancino, M. Hocevar, D. Bozic, A. Bedina Zavec, M. Podobnik, M.P. Stoppelli, A. Kisslinger, A. Bongiovanni, V. Kralj-Iglic, G.L. Liguori, A novel localization in human large extracellular vesicles for the EGF-CFC founder member CRIPTO and its biological and therapeutic implications, Cancers 14 (2022).
[51] Y. Azuma, A. Nakaya, S. Fujita, A. Satake, T. Nakanishi, Y. Tsubokura, R. Saito, A. Konishi, M. Hotta, H. Yoshimura, Neutrophil-to-lymphocyte ratio (NLR) fails to predict outcome of diffuse large B cell lymphoma, Leuk. Res. Rep. 12 (2019) 100173.
[52] E.M. Lauer, J. Mutter, F. Scherer, Circulating tumor DNA in B-cell lymphoma: technical advances, clinical applications, and perspectives for translational research, Leukemia 36 (2022) 2151–2164.
[53] Y. Lévy, A. Wiedemann, B.P. Hejblum, M. Durand, C. Lefebvre, M. Surénaud, C. Lacabaratz, M. Perreau, E. Foucat, M. Déchenaud, CD177, a specific marker of neutrophil activation, is associated with coronavirus disease 2019 severity and death, Iscience 24 (2021).
[54] S. Mu, L. Ai, F. Fan, Y. Qin, C. Sun, Y. Hu, Prognostic role of neutrophil-to-lymphocyte ratio in diffuse large B cell lymphoma patients: an updated dose–response meta-analysis, Cancer Cell Int. 18 (2018) 1–9.
[55] J.S. Heitmann, I. Hagelstein, C. Hinterleitner, L. Osburg, H.R. Salih, J. Kauer, M. Märklin, Fc gamma receptor expression serves as prognostic and diagnostic factor in AML, Leuk. Lymphoma 61 (2020) 2466–2474.
[56] M.W. Fanger, L. Shen, R.F. Graziano, P.M. Guyre, Cytotoxicity mediated by human Fc receptors for IgG, Immunol. Today 10 (1989) 92–99.
[57] E.I. Buzas, The roles of extracellular vesicles in the immune system, Nat. Rev. Immunol. 23 (2023) 236–250.
[58] G. Cetin, S. Klafack, M. Studencka-Turski, E. Kruger, F. Ebstein, The ubiquitin-proteasome system in immune cells, Biomolecules 11 (2021).
[59] H. Yu, L. Lin, Z. Zhang, H. Zhang, H. Hu, Targeting NF-κB pathway for the therapy of diseases: mechanism and clinical study, Signal Transduct. Target. Ther. 5 (2020) 209.

[60] W.L. Lee, M.-K. Kim, A.D. Schreiber, S. Grinstein, Role of ubiquitin and proteasomes in phagosome maturation, Mol. Biol. Cell 16 (2005) 2077–2090.
[61] D. Ichikawa, M. Mizuno, T. Yamamura, S. Miyake, GRAIL (gene related to anergy in lymphocytes) regulates cytoskeletal reorganization through ubiquitination and degradation of Arp2/3 subunit 5 and coronin 1A, J. Biol. Chem. 286 (2011) 43465–43474.
[62] H. Hu, S.-C. Sun, Ubiquitin signaling in immune responses, Cell Res. 26 (2016) 457–483.
[63] C. Madiraju, J.P. Novack, J.C. Reed, S.I. Matsuzawa, K63 ubiquitination in immune signaling, Trends Immunol. 43 (2) (2022) 148–162, https://doi.org/10.1016/j.it.2021.12.005. Epub 2022 Jan 13. PMID: 35033428; PMCID: PMC8755460.
[64] H.X. Liao, X. Mao, L. Wang, N. Wang, D.K.W. Ocansey, B. Wang, F. Mao, The role of mesenchymal stem cells in attenuating inflammatory bowel disease through ubiquitination, Front. Immunol. 15 (2024) 1423069.
[65] M. Liang, X. Chen, L. Wang, L. Qin, H. Wang, Z. Sun, W. Zhao, B. Geng, Cancer-derived exosomal TRIM59 regulates macrophage NLRP3 inflammasome activation to promote lung cancer progression, J. Exp. Clin. Cancer Res. 39 (2020) 1–17.
[66] B. Mirlekar, Y. Pylayeva-Gupta, IL-12 family cytokines in cancer and immunotherapy, Cancers 13 (2021).
[67] E.W. Deutsch, N. Bandeira, V. Sharma, Y. Perez-Riverol, J.J. Carver, D.J. Kundu, D. García-Seisdedos, A.F. Jarnuczak, S. Hewapathirana, B.S. Pullman, The ProteomeXchange consortium in 2020: enabling 'big data' approaches in proteomics, Nucleic Acids Res. 48 (2020) D1145–D1152.
[68] Y. Perez-Riverol, A. Csordas, J. Bai, M. Bernal-Llinares, S. Hewapathirana, D. J. Kundu, A. Inuganti, J. Griss, G. Mayer, M. Eisenacher, The PRIDE database and related tools and resources in 2019: improving support for quantification data, Nucleic Acids Res. 47 (2019) D442–D450.